




Single-photon peak event detection (SPEED): a computational method for fast photon counting in fluorescence lifetime imaging microscopy: supplement

JANET E. SORRELLS,^{1,2}  RISHYASHRING R. IYER,^{1,3}  LINGXIAO YANG,^{1,3}  ERIC J. CHANEY,¹ MARINA MARJANOVIC,^{1,2,4} HAOHUA TU,^{1,3} AND STEPHEN A. BOPPART^{1,2,3,4,5,*} 

¹Beckman Institute for Advanced Science and Technology, University of Illinois at Urbana-Champaign, Urbana, IL 61801, USA

²Department of Bioengineering, University of Illinois at Urbana-Champaign, Urbana, IL 61801, USA

³Department of Electrical and Computer Engineering, University of Illinois at Urbana-Champaign, Urbana, IL 61801, USA

⁴Carle Illinois College of Medicine, University of Illinois at Urbana-Champaign, Urbana, IL 61801, USA

⁵Cancer Center at Illinois, Urbana, IL 61801, USA

*boppart@illinois.edu

This supplement published with Optica Publishing Group on 29 October 2021 by The Authors under the terms of the [Creative Commons Attribution 4.0 License](https://creativecommons.org/licenses/by/4.0/) in the format provided by the authors and unedited. Further distribution of this work must maintain attribution to the author(s) and the published article's title, journal citation, and DOI.

Supplement DOI: <https://doi.org/10.6084/m9.figshare.16837840>

Parent Article DOI: <https://doi.org/10.1364/OE.439675>

Single-photon peak event detection (SPEED): A computational method for fast photon counting in fluorescence lifetime imaging microscopy

JANET E. SORRELLS^{1,2}, RISHYASHRING R. IYER^{1,3}, LINGXIAO YANG^{1,3}, ERIC J. CHANEY¹, MARINA MARJANOVIC^{1,2,4}, HAOHUA TU^{1,3}, AND STEPHEN A. BOPPART^{1,2,3,4,5,*}

¹Beckman Institute for Advanced Science and Technology, University of Illinois at Urbana-Champaign, Urbana, IL, 61801, USA

²Department of Bioengineering, University of Illinois at Urbana-Champaign, Urbana, IL, 61801, USA

³Department of Electrical and Computer Engineering, University of Illinois at Urbana-Champaign, Urbana, IL, 61801, USA

⁴Carle Illinois College of Medicine, University of Illinois at Urbana-Champaign, Urbana, IL, 61801, USA

⁵Cancer Center at Illinois, Urbana, IL, 61801, USA

*boppart@illinois.edu

© 2021 Optical Society of America under the terms of the [OSA Open Access Publishing Agreement](#)

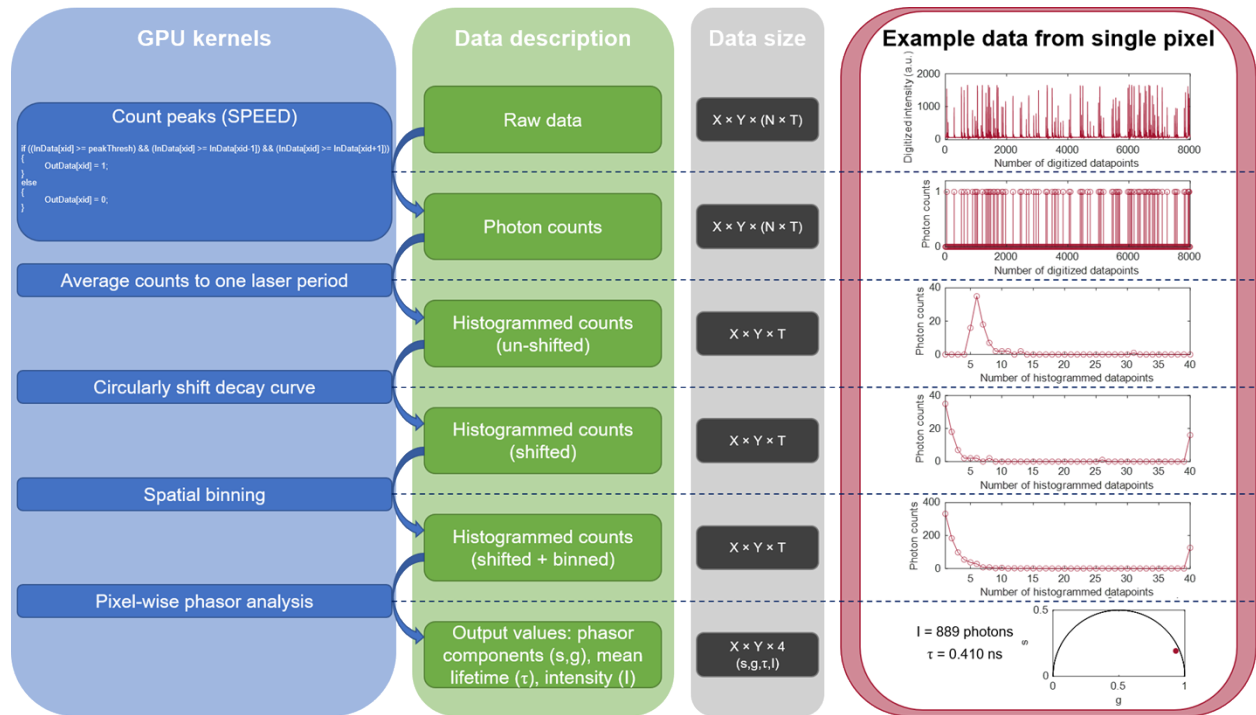


Fig. S1. Flowchart of graphics processing unit (GPU) analysis steps from directly digitized raw data to output intensity (I), lifetime (τ), and phasor components (s, g). Photon counting using SPEED is performed in the first kernel (“Count peaks”), where each digitized datapoint is classified as a photon count if it is above the peak threshold ($peakThreshold$) and greater than the datapoint immediately before and after it. Following photon counting, photon counts for each pixel are histogrammed into a plot of photon counts vs. time bin (“Average counts to one laser period”), shifted so that the maximum value falls at time = 0 ns (“Circularly shift decay curve”), spatially binned with neighboring pixels (“Spatial binning”), and then pixel-wise phasor analysis is performed to compute the output lifetime and phasor components. X , number of pixels in X ; Y , number of pixels in Y ; N , number of laser pulses per pixel ($N = 200$ for example pixel); T , number of digitized datapoints per pixel ($T = 40$ for example pixel); $InData$, raw directly digitized data; $OutData$, photon counts.

Table S1. Single frame acquisition and processing timing.

Method	Direct pulse sampling [1]	SPEED
Raw data dimensions ($x \times y \times t$)	$256 \times 256 \times 16000$	$256 \times 256 \times 16000$
Raw data size (MB)	2097.15	2097.15
Processed data size (MB)	0.79	5.75
Processed data files and dimension	Intensity (256×256) Mean lifetime (256×256) g (256×256) s (256×256) N/A	Intensity (256×256) Mean lifetime (256×256) g (256×256) s (256×256) Fluorescence decay ($256 \times 256 \times 40$)
Pixel rate (MHz)	0.2	0.2
Frame acquisition time (ms)	1639.34	1639.34
Host to device memory copying time (ms)	459.90	459.90
Device to host memory copying time (ms)	0.06	0.66
GPU all kernels processing time (ms)	66.20	88.82
Kernel: “Peak detection” processing time (ms)	N/A	51.58
Kernel: “Average to a single decay curve” processing time (ms)	63.16	33.99
Total processing + data copying time (ms)	526.16	539.78

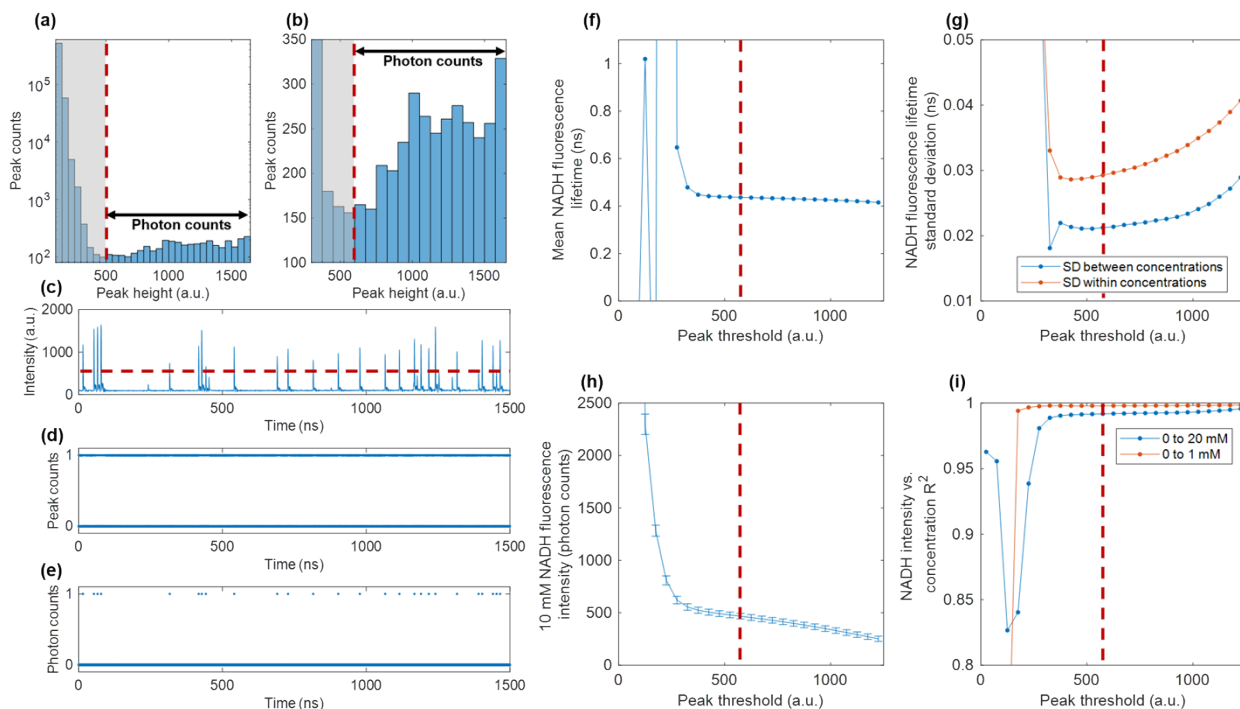


Fig. S2. Photon peak discrimination threshold determination. (a) Logarithmic histogram of number of detected peaks in digitized data and the values of those peaks, in arbitrary units. Peaks, digitized datapoints that were higher than the datapoints immediately before and after it, were determined from raw digitized data from 2 mM NADH in solution. (b) Zoomed-in non-logarithmic histogram focused on region with peaks corresponding to photon counts. The excess noise factor (F_e), was calculated as the normalized second moment of the photon count peak height distribution [2], and was determined to be approximately 1.25. The experimentally determined minimum photon peak height for our setup (575 a.u.), which is dependent on the PMT control voltage, amplifier, digitizer DC offset, and any normalization on digitized data, is indicated with a red dashed line. Datapoints with a peak height above this value are considered photon counts by our SPEED algorithm. (c) Example intensity over time of raw digitized data, with the red dashed threshold for photon counts. All peaks from (c) are shown in (d), and all photon counts from (c) are shown in (e). To determine the effect of changing the peak discrimination threshold, thresholds from 25 to 1225 a.u. were examined for (f) NADH fluorescence lifetime accuracy, (g) fluorescence lifetime standard deviation, (h) intensity, (i) and linear dependence of intensity on concentration. From (a) and (b), it is clear that somewhere from 475-675 a.u. is a reasonable peak discrimination threshold, with the minimum value falling at 575 a.u.; clearly, peak discrimination thresholds below around 400 a.u. are highly susceptible to counting false peaks and do not produce accurate or precise results. In (h), there is a 10.2% difference between the NADH intensity in photon counts calculated using 475 and 675 a.u. as the peak discrimination threshold. As the threshold goes to higher values, more photon peaks are missed, and as the threshold goes to lower values, more noise peaks are classified as photon counts. With fewer photons counted, the fluorescence lifetime standard deviation (g) increases as the peak threshold increases. The calculated fluorescence lifetime (f) and R^2 values for a linear fit between intensity (in photon counts) and NADH concentration (i) are very robust and do not have a large dependence on the peak discrimination threshold; this is because if $\sim 10\%$ of photon peaks are missed due to a high threshold, the mean fluorescence lifetime will still work out to be similar on average, and the intensity will just decrease by $\sim 10\%$ for each concentration, maintaining linearity.

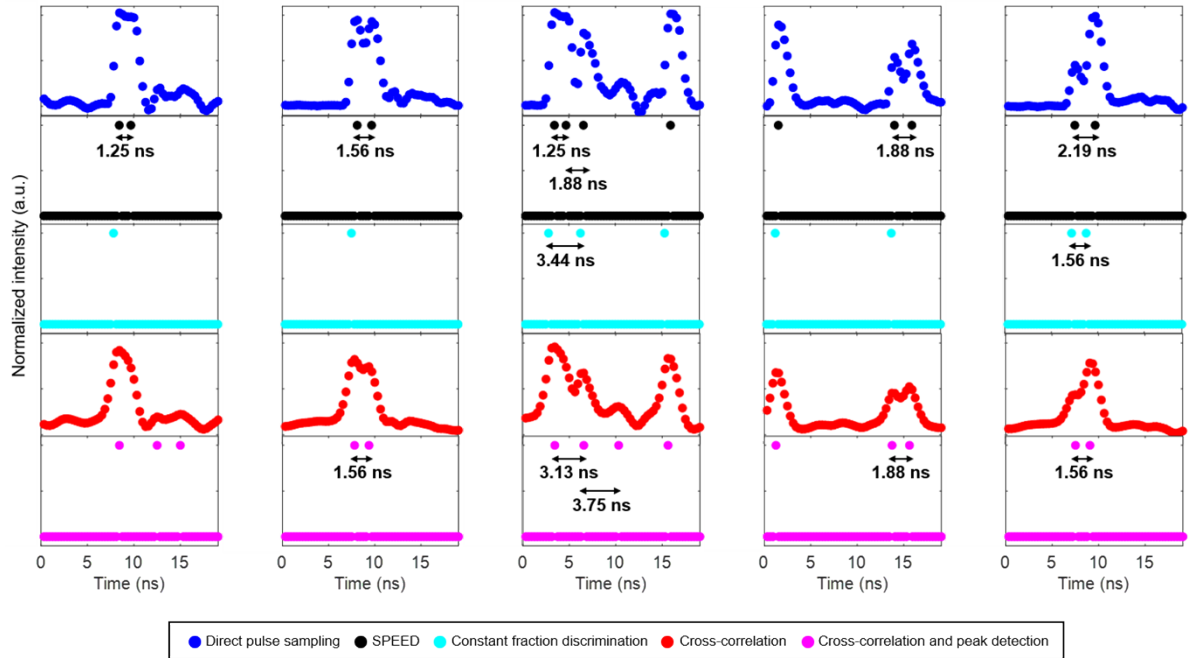


Fig. S3. Computational single-photon counting methods on five segments of representative raw data where consecutive photons arrived within several ns. Five computational analysis techniques performed on the same set of digitized data: direct pulse sampling (blue), SPEED (black), constant fraction discrimination (cyan), cross-correlation with direct pulse sampling IRF (red), and cross-correlation with direct pulse sampling IRF followed by peak detection (magenta). SPEED provides the smallest and most reliable temporal resolution. Both CFD and cross-correlation with peak detection were unable to resolve distinct photon arrivals separated by less than 1.56 ns. CFD additionally tended to undercount some photons separated by less than 2 ns, and cross-correlation with peak detection tended to overcount bumps from the system IRF as photons arrivals.

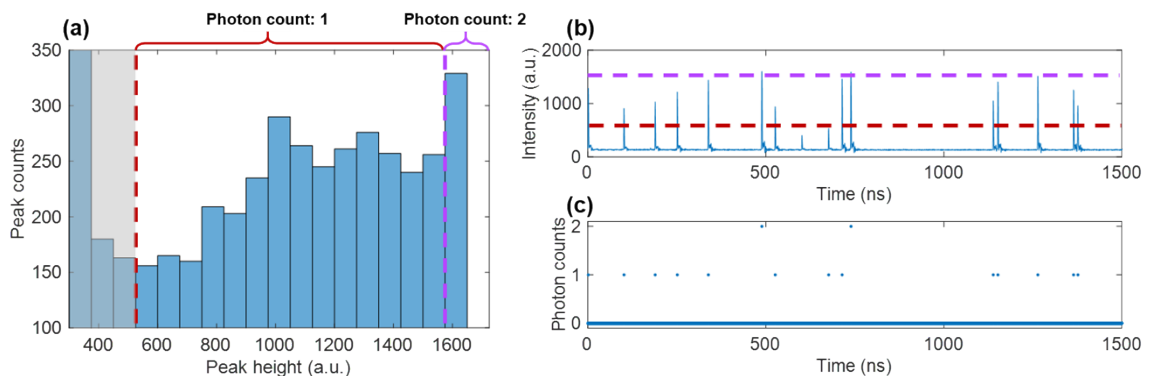


Fig. S4. Photon peak discrimination with a dual-threshold model. (a) Zoomed-in histogram focused on region with peaks corresponding to one photon count (550 a.u. to 1575 a.u.) and two photon counts (about 1575 a.u.). Similar to Fig. S1, the experimentally determined minimum peak threshold for a single photon count is represented by the red dashed line, and additionally a second threshold for a photon count of two is given by the purple dashed line. (b) Example intensity over time of raw digitized data, with the single (red) and double (purple) photon thresholds. (c) Photon counts from (b).

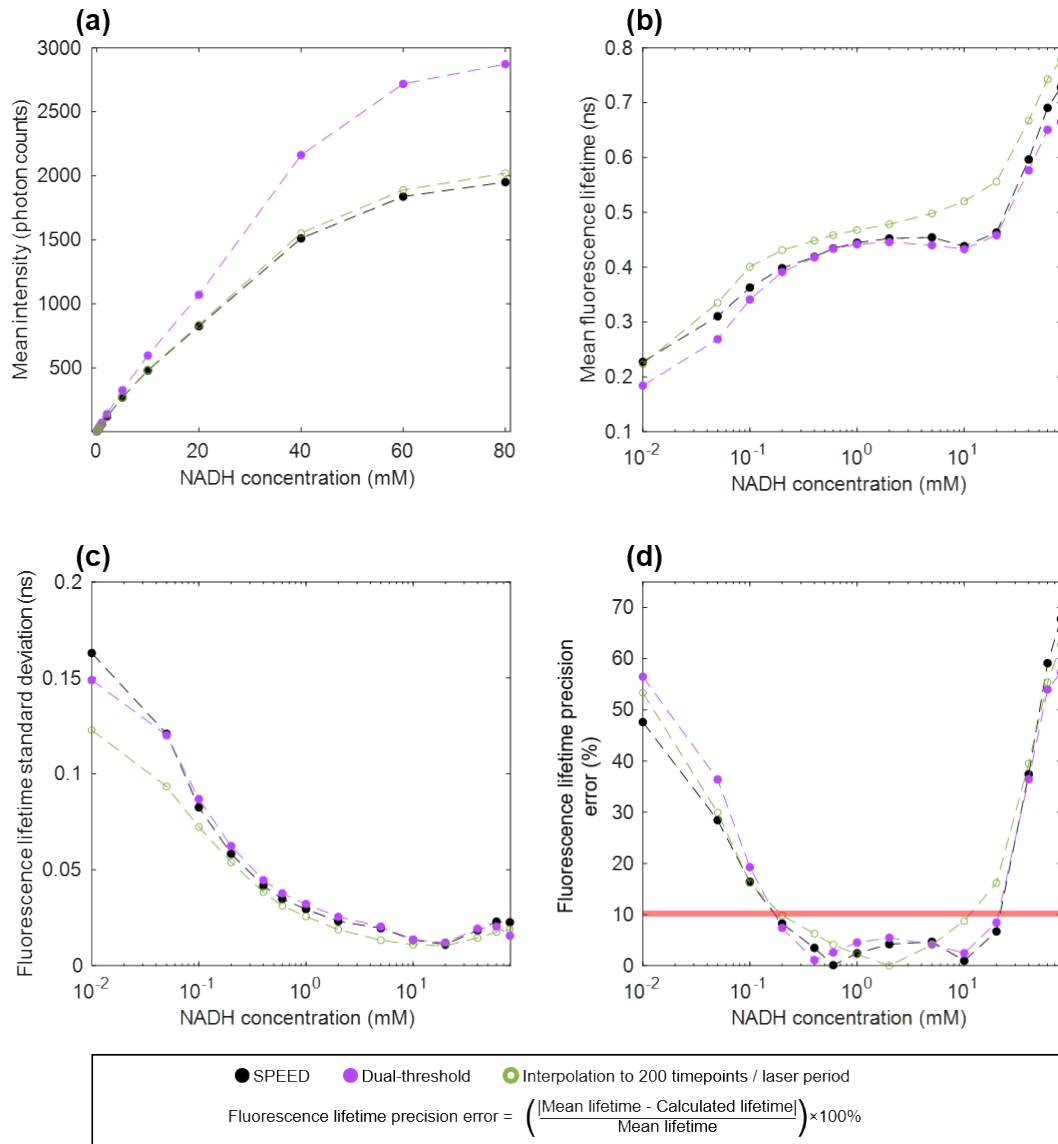


Fig. S5. Intensity linearity, fluorescence lifetime accuracy, and fluorescence lifetime precision, and characterization of fluorescence lifetime error using SPEED, with dual-threshold photon counting and interpolation, for concentrations of NADH from 0.01 mM to 80 mM. (a) Mean pixel intensity estimated using SPEED with no interpolation of raw data and only one threshold for photon counts (black), SPEED with a dual threshold for photon counts (purple), and SPEED with interpolation of raw data to 200 timepoints per laser period (green). (b) Mean pixel fluorescence lifetime, (c) pixel fluorescence lifetime standard deviation, and (d) fluorescence lifetime precision error using the three indicated SPEED methods. The mean fluorescence lifetime in the regions of each technique with approximately linear intensity was determined (SPEED: 0.05 mM to 20 mM, mean lifetime = 0.434 ns; dual-threshold: 0.05 mM to 20 mM, mean lifetime = 0.422 ns; interpolation: 0.05 mM to 20 mM, mean lifetime = 0.478 ns).

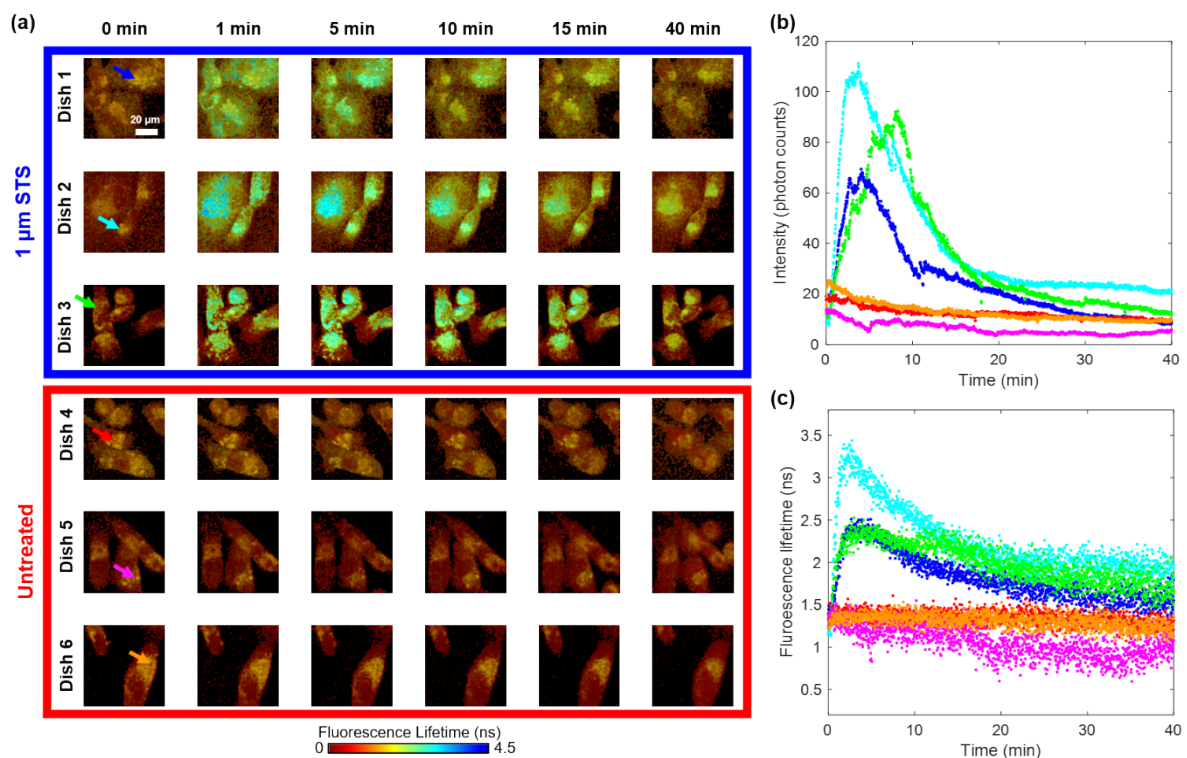


Fig. S6. Dynamics of NAD(P)H in staurosporine-induced apoptosis in human breast cancer cells (MDA-MB-231). (a) Select frames from each dish at 6 different timepoints. Each image is the average of five consecutive frames, and displays the gamma-corrected intensity-weighted fluorescence lifetime, with a gamma of 0.35. One 11 \times 11 pixel mitochondria area was selected from each dish, indicated by the arrows, and the (b) intensity and (c) lifetime for that mitochondria area is shown as well.

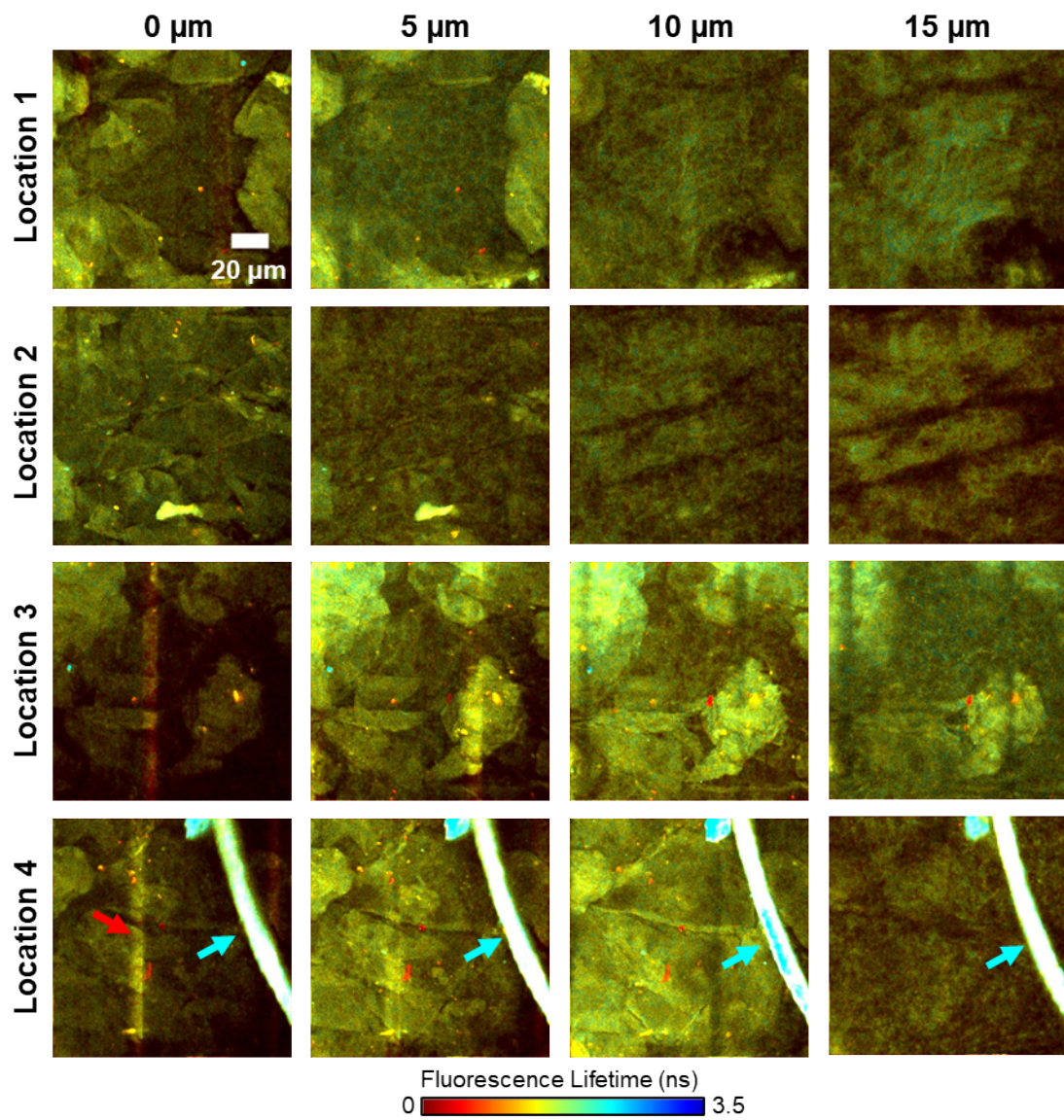


Fig. S7. *In vivo* imaging of murine skin. Four different locations were imaged, and for each one we examined the outer *stratum corneum* and then acquired a z-stack of images to examine the more interior *stratum granulosum*. Breathing artifacts from the animal are visible (red arrow) as well as a hair in location 4 (cyan arrows). Each image is an average of four 512 \times 512 images.

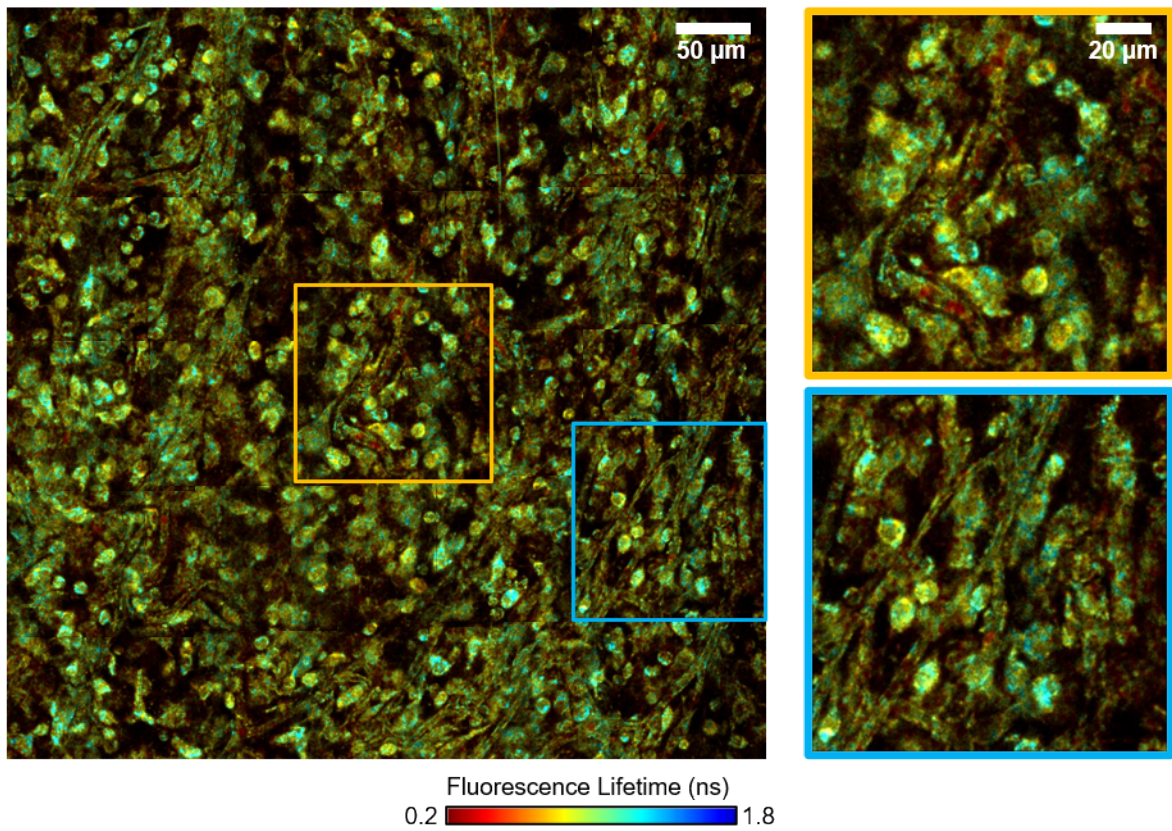


Fig. S8. *Ex vivo* rat mammary tumor mosaic. A 5×5 mosaic was acquired $20 \mu\text{m}$ deep into the tumor tissue sample, with each tile acquired as an average of four 512×512 pixel, $128 \times 128 \mu\text{m}$ images. Two tiles, outlined in yellow and light blue are shown on the right on a larger scale. Individual cells and fibers can be resolved throughout the mosaic.

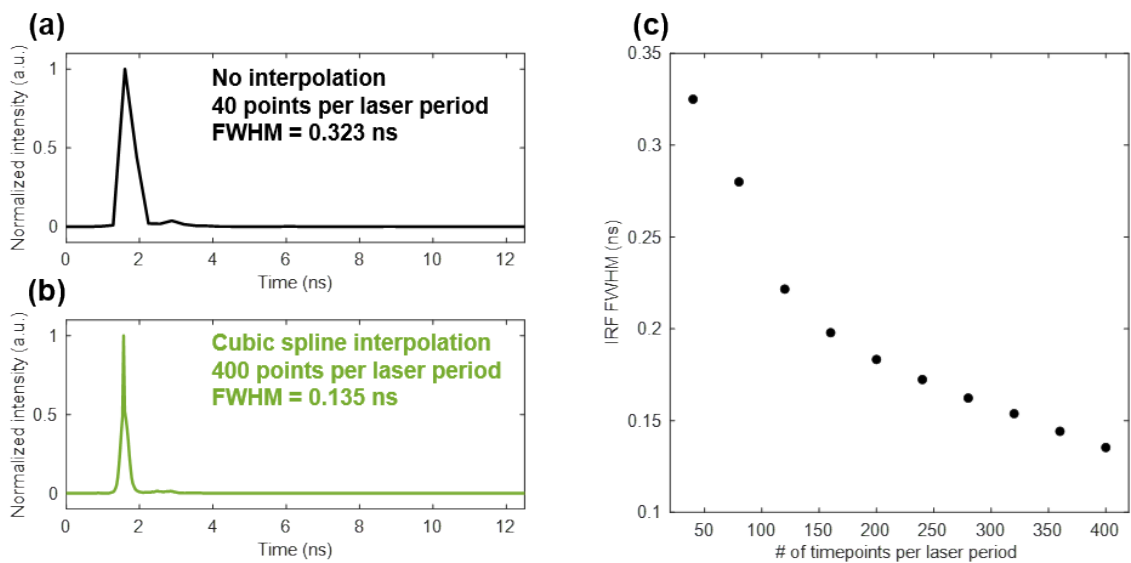


Fig. S9. Impulse response function (IRF), calculated as the average pixel decay resultant from imaging second harmonic generation from a BBO crystal using SPEED and with cubic spline interpolation, performed on the same set of digitized data as in Fig. 2 from the main text. (a) SPEED IRF calculated without interpolation, with a full width at half-maximum (FWHM) of 0.323 ns . (b) SPEED IRF calculated with cubic spline interpolation on raw data to increase the number of points per laser period from 40 to 400, with a FWHM of 0.135 ns . (c) IRF FWHM calculated based on the number of timepoints per laser period in raw data interpolated with cubic spline.

REFERENCES

1. J. E. Sorrells, R. R. Iyer, L. Yang, A. J. Bower, D. R. Spillman, E. J. Chaney, H. Tu, M. Marjanovic, S. A. Boppart, "Real-time pixelwise phasor analysis for video-rate two-photon fluorescence lifetime imaging microscopy," *Biomed. Opt. Express* **12**(7), 4003 – 4019 (2021).
2. M. C. Teich, K. Matsuo, B. E. A. Saleh, "Excess noise factors for conventional and superlattice avalanche photodiodes and photomultiplier tubes," *IEEE J. Quantum Electron.* **QE-22**(8), 1184 – 1193 (1986).